Influence of magnetic anisotropy on the Kondo effect and spin-polarized transport through magnetic molecules, adatoms, and quantum dots

Maciej Misiorny,[1,*] Ireneusz Weymann,[1,2] and Józef Barnaś[1,3]

[1]*Faculty of Physics, Adam Mickiewicz University, PL-61-614 Poznań, Poland*

[2]*Physics Department, Arnold Sommerfeld Center for Theoretical Physics and Center for NanoScience, Ludwig-Maximilians-Universität München, D-80333 München, Germany*

[3]*Institute of Molecular Physics, Polish Academy of Sciences, PL-60-179 Poznań, Poland*

Transport properties in the Kondo regime of a nanosystem displaying uniaxial magnetic anisotropy (such as a magnetic molecule, magnetic adatom, or quantum dot coupled to a localized magnetic moment) are analyzed theoretically. In particular, the influence of spin-polarized transport through a local orbital of the system and exchange coupling of conduction electrons to the system's magnetic core on the Kondo effect is discussed. The numerical renormalization-group method is applied to calculate the spectral functions and linear conductance in the case of the parallel and antiparallel configurations of the electrodes' magnetic moments. It is shown that both the magnetic anisotropy as well as the exchange coupling between electrons tunneling through the conducting orbital and magnetic core play an important role in the formation of the Kondo resonance, leading generally to its suppression. Specific transport properties of such a system appear also as a nontrivial behavior of tunnel magnetoresistance. It is also shown that the Kondo effect can be restored by an external magnetic field in both the parallel and antiparallel magnetic configurations.

PACS number(s): 72.25.−b, 75.50.Xx, 85.75.−d

I. INTRODUCTION

The growing trend toward building ever more efficient and smaller electronic devices inevitably draws the researchers' attention to nanoscopic hybrid systems. In this respect, single atoms or molecules seem to be promising prospects, as their incorporation into electronic nanodevices allows for developing novel systems capable of performing strictly imprinted functions,[1–6] among which information storage is of key interest.[7–10] Consequently, due to recent advances in experimental techniques enabling us to address transport through individual atoms and molecules, both natural as well as artificial (quantum dots) systems exhibiting magnetic anisotropy, such as magnetic atoms of spin $S > 1/2$ (i.e., Fe, Co, or Mn)[9,11–15] or single-molecule magnets (SMMs),[16–20] have become the object of intensive studies.

It has been suggested, and in the case of magnetic adatoms also experimentally proven,[9] that the magnetic state of such systems can by controlled by the use of spin-polarized currents[21–26] or spin bias.[27] This practically means that the system's magnetic moment can be switched between two metastable states of minimal energy by only applying an electric/spin current pulse of a proper amplitude.[24] Furthermore, if attached to two metallic nonmagnetic electrodes a SMM can act as a spin filter.[28–30] If, however, coupled to electrodes characterized by unequal spin polarizations, the molecule can reveal transport characteristics typical of a spin diode.[31] Most of these results have been obtained in the limit of weak coupling between a SMM and reservoirs of spin-polarized electrons. Nevertheless, in some situations, when mixing of localized electron states responsible for transport properties of the molecule and extended electron states in electrodes is significant, such an assumption does not necessarily have to be correct.

In the strong-coupling regime the electronic correlations can lead to an additional resonance in the density of states at the Fermi level of electrodes, known as the *Kondo-Abrikosov-Suhl resonance*.[32–34] Since the end of the 1990s, the presence of the Kondo effect has been successively demonstrated in a large variety of nanoscopic objects like quantum dots,[35–37] magnetic adatoms,[38,39] nanotubes,[40] and different types of molecules: Co(II)-based coordination complexes;[41] divanadium molecules;[42] and C_{60} molecules attached to gold[43] or ferromagnetic nickel electrodes.[44] However, in the case of nanosystems characterized by large spins, the prominent role of the magnetic anisotropy in the formation of the Kondo effect has been experimentally established only very recently.[14,45] It turned out that the Kondo effect can be then tuned by changing both the orientation (e.g., by controlling the adatom's local environment[14]) and magnitude (e.g., by mechanical straining of the molecule[45]) of the magnetic anisotropy. Moreover, Parks *et al.*[45] were able to tune the anisotropy constant continuously and to modify accordingly the energy spectrum underlying the Kondo state. As a result, they managed to observe a crossover from the fully screened to underscreened Kondo effect. It is worthy of note that more recently electric-field control of magnetic anisotropy has been experimentally established for a SMM embedded into a planar three-terminal device.[20] Although a few theoretical works focused on transport related issues in SMMs in the Kondo regime have been already published,[46–53] experimental evidence of the Kondo effect in transport through SMMs has been found only very recently.[20]

The earlier works on the Kondo phenomenon in transport through SMMs have been primarily focused on the role of transversal magnetic anisotropy, and hence also on the role of quantum tunneling of the SMM's spin in the formation of the Kondo state. It has been shown that the interplay of quantum tunneling and spin-exchange processes between the molecule and tunneling electrons may result in the pseudo-spin-1/2 Kondo effect.[46,47] Furthermore, it was soon realized that when even a moderate transverse magnetic field is applied, any qualitative difference between the mechanisms of the Kondo

effect for molecules with half- and full-integer spins cease to exist.[48] Mapping of the Anderson-type Hamiltonian describing a SMM onto the spin-1/2 anisotropic Kondo Hamiltonian[49] led to the conclusion that, depending on whether the molecule's total spin is reduced or augmented in the singly charged state, the coupling in the Kondo Hamiltonian is antiferromagnetic or ferromagnetic, respectively. In the former case the Kondo effect is revealed, whereas in the latter one no resonance at the Fermi level is present due to renormalization of the transverse coupling to zero. In addition, the Kondo effect is expected to oscillate as a function of the magnitude of transverse field due to the Berry-phase periodical modulation of the tunnel splitting.[48] Finally, the nonequilibrium spin dynamics of a SMM, triggered by a sudden change in the magnetic-field amplitude has been studied, with the main emphasis on the time evolution of the Kondo screening.[50]

Since physical mechanisms governing Kondo correlations in spin-polarized transport through nanoscopic systems exhibiting the magnetic anisotropy, such as magnetic adatoms or SMMs, are still at the early stage of research, the objective of the present paper is to provide further insight into the problem. In particular, we investigate how magnetic anisotropy affects the system's transport characteristics such as conductance and tunnel magnetoresistance (TMR) in the linear-response regime. To properly describe the transport properties in the strong-coupling regime, we employ the Wilson's numerical renormalization-group (NRG) approach.[32,54,55] This method is known as very powerful and essentially exact in solving quantum impurity problems.

The paper is organized as follows. In Sec. II we describe the model Hamiltonian used in calculations and provide a brief introduction to the NRG method. Numerical results and their discussion are given in Sec. III, where we analyze the spectral functions of the orbital level as well as the conductance and tunnel magnetoresistance (TMR) in the linear-response regime. The above quantities are analyzed as functions of the orbital level position, strength, and type of exchange coupling, and the anisotropy constant. In addition, we also discuss the effect of external magnetic field. Finally, the summary and conclusions are given in Sec. IV.

II. THEORETICAL DESCRIPTION

A. Model

We consider a generic theoretical model that allows for capturing essential features of quantum objects such as magnetic adatoms, quantum dots coupled to localized magnetic moments, and SMMs; see Fig. 1. It is assumed that electronic transport takes place *via* a single local orbital level (OL) of the system (conducting orbital of a SMM, adatom, or quantum dot), which is coupled to electrodes. Moreover, the OL is also exchange-coupled to the corresponding magnetic core. Without loss of generality, we will henceforth refer to the systems under investigation as *magnetic quantum dots* (MQDs).

The total Hamiltonian of a MQD coupled to external leads can be written as

$$\mathcal{H} = \mathcal{H}_{\text{MQD}} + \mathcal{H}_{\text{leads}} + \mathcal{H}_{\text{tun}}. \tag{1}$$
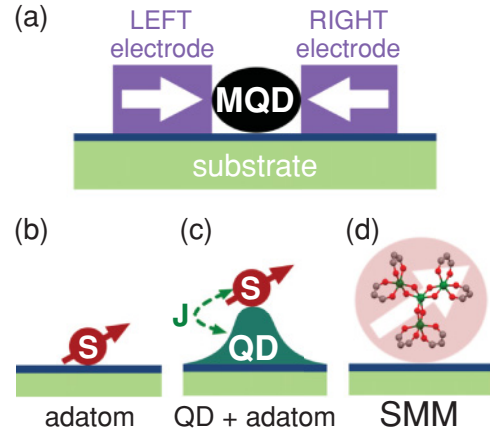

FIG. 1. (Color online) (a) Schematic representation of the system under consideration. The system consists of two ferromagnetic electrodes to which a magnetic quantum dot (MQD) exhibiting magnetic anisotropy is attached. As the MQD one can conceive either (b) a magnetic adatom (i.e., Fe, Co, Mn), (c) semiconductor quantum dot coupled to a magnetic moment, or (d) a single-molecule magnet (SMM)—here, only the magnetic core of the Fe₄ molecule (Ref. 56) is schematically depicted.

The first term represents the MQD and has the form[21–25]

$$\mathcal{H}_{\text{MQD}} = -D S_z^2 + \sum_{\sigma=\uparrow,\downarrow} \varepsilon\, n_\sigma + U\, n_\uparrow n_\downarrow$$
$$- J\mathbf{s} \cdot \mathbf{S} + B_z(S_z + s_z), \tag{2}$$

where D stands for the uniaxial anisotropy constant of the MQD, while S_z denotes the zth component of the MQD's internal spin operator $\mathbf{S}$. Since in the present paper we focus only on systems displaying magnetic bistability, the anisotropy constant is assumed to be positive ($D > 0$). Furthermore, $n_\sigma = c_\sigma^\dagger c_\sigma$ is the OL occupation operator, where $c_\sigma^\dagger (c_\sigma)$ creates (annihilates) a spin-σ electron of energy ε in the OL. The Coulomb energy of two electrons of opposite spins occupying the OL is given by U. The penultimate term of Eq. (2) accounts for exchange coupling between the magnetic core of a MQD and the spin of an electron in the OL, represented by $\mathbf{s} = \frac{1}{2}\sum_{\sigma\sigma'} c_\sigma^\dagger \boldsymbol{\sigma}_{\sigma\sigma'} c_{\sigma'}$, where $\boldsymbol{\sigma} \equiv (\sigma^x, \sigma^y, \sigma^z)$ is the Pauli spin operator. The J coupling can be either of *ferromagnetic* ($J > 0$) or *antiferromagnetic* ($J < 0$) type. Finally, the last term of Eq. (2) describes the Zeeman interaction of the MQD with an external magnetic field $\mathbf{B} = (0,0,B_z)$ oriented along the easy axis of a MQD. Note that we put here $g\mu_{\text{B}} \equiv 1$.

The ferromagnetic metallic electrodes, to which a MQD is coupled through the OL, are characterized by noninteracting itinerant electrons with the dispersion relation $\varepsilon_{\mathbf{k}\sigma}^q$, where q indicates either the left ($q = L$) or right ($q = R$) electrode, $\mathbf{k}$ denotes a wave vector, and σ is a spin index of an electron. Thus the leads' Hamiltonian is given by

$$\mathcal{H}_{\text{leads}} = \sum_{q=L,R} \sum_{\mathbf{k}} \sum_{\sigma=\uparrow,\downarrow} \varepsilon_{\mathbf{k}\sigma}^q a_{\mathbf{k}\sigma}^{q\dagger} a_{\mathbf{k}\sigma}^q, \tag{3}$$

with $a_{\mathbf{k}\sigma}^{q\dagger} (a_{\mathbf{k}\sigma}^q)$ being the relevant electron creation (annihilation) operator. At this point, it should also be mentioned that in the present paper we limit the discussion to collinear (parallel and antiparallel) configurations of electrodes' magnetic

moments. Furthermore, the MQD's easy axis is assumed to be collinear with these moments as well. Finally, electron tunneling processes between the MQD and electrodes are included in the term $\mathcal{H}_{\text{tun}}$,

$$\mathcal{H}_{\text{tun}} = \sum_{q=L,R} \sum_{\mathbf{k}} \sum_{\sigma=\uparrow,\downarrow} T_{\mathbf{k}\sigma}^{q} a_{\mathbf{k}\sigma}^{q\dagger} c_{\sigma} + \text{H.c.,} \quad (4)$$

where $T_{\mathbf{k}\sigma}^{q}$ denotes the tunnel matrix element between the OL and the qth lead.

In the linear-response regime, it is numerically convenient to introduce the following canonical transformation:[57–59]

$$\begin{pmatrix} a_{\mathbf{k}\sigma}^{e} \\ a_{\mathbf{k}\sigma}^{o} \end{pmatrix} = \frac{1}{\mathcal{V}_{\mathbf{k}\sigma}} \begin{pmatrix} T_{\mathbf{k}\sigma}^{L} & T_{\mathbf{k}\sigma}^{R} \\ -T_{\mathbf{k}\sigma}^{R} & T_{\mathbf{k}\sigma}^{L} \end{pmatrix} \begin{pmatrix} a_{\mathbf{k}\sigma}^{L} \\ a_{\mathbf{k}\sigma}^{R} \end{pmatrix}, \quad (5)$$

where $\mathcal{V}_{\mathbf{k}\sigma} = \sqrt{|T_{\mathbf{k}\sigma}^{L}|^{2} + |T_{\mathbf{k}\sigma}^{R}|^{2}}$, and the label e (o) denotes the even (odd) combination of the leads operators. Such a rotation in the space of the left-right electron operators results in the separation of the total Hamiltonian, Eq. (1), into two independent parts. The first one involves the OL coupled to a single electron reservoir described by the even linear combination of the leads' electron operators, $a_{\mathbf{k}\sigma}^{e}$, while the other one is related with noninteracting electrons decoupled from MQD and described by the odd operators $a_{\mathbf{k}\sigma}^{o}$. Consequently, the tunneling Hamiltonian can be written as

$$\mathcal{H}_{\text{tun}} = \sum_{\mathbf{k}} \sum_{\sigma=\uparrow,\downarrow} \mathcal{V}_{\mathbf{k}\sigma} \left[a_{\mathbf{k}\sigma}^{e\dagger} c_{\sigma} + c_{\sigma}^{\dagger} a_{\mathbf{k}\sigma}^{e} \right], \quad (6)$$

with $\mathcal{V}_{\mathbf{k}\sigma}$ being effective OL-lead tunneling matrix elements. In the following we assume that the full spin dependence is taken into account through the matrix elements $\mathcal{V}_{\mathbf{k}\sigma}$.[60,61] For simplicity, we assume a flat conduction band in the interval $[-W,W]$, so that $\rho_{\sigma}(\omega) \equiv \rho = \frac{1}{2W}$, with W representing the cutoff energy of the system and $W \equiv 1$ taken as the energy unit. Finally, the energy dependence of $\mathcal{V}_{\mathbf{k}\sigma}$ is neglected, $\mathcal{V}_{\mathbf{k}\sigma} \equiv \mathcal{V}_{\sigma}$.[62] Under these circumstances, the overall effect of the ferromagnetic reservoir on the MQD is completely determined by the hybridization function Γ_{σ},

$$\Gamma_{\sigma} = \pi\rho|\mathcal{V}_{\sigma}|^{2}. \quad (7)$$

B. Method of calculations

In order to determine transport properties in the strong-coupling regime, we use Wilson's numerical renormalization-group method.[32,54,55] The NRG technique consists of logarithmic discretization of the conduction band (with a discretization parameter $\Lambda > 1$) into intervals $[\Lambda^{-(n+1)}W, \Lambda^{-n}W]$ and $[-\Lambda^{-n}W, -\Lambda^{-(n+1)}W]$ for $n = 0,1,2,3,\ldots$, which allows for resolving transport properties on energy scales logarithmically approaching the Fermi level. After having discretized the conduction band, such a model is mapped onto a semi-infinite chain, whose first site is coupled to the impurity (in our case the MQD). The Hamiltonian then reads[32,55]

$$\mathcal{H} = \mathcal{H}_{\text{MQD}} + \sum_{\sigma=\uparrow,\downarrow} \sqrt{\frac{\Gamma_{\sigma}}{\pi\rho}} [c_{\sigma}^{\dagger} f_{0\sigma} + f_{0\sigma}^{\dagger} c_{\sigma}]$$
$$+ \sum_{n=0}^{\infty} \sum_{\sigma=\uparrow,\downarrow} t_{n} [f_{n\sigma}^{\dagger} f_{n+1\sigma} + f_{n+1\sigma}^{\dagger} f_{n\sigma}]. \quad (8)$$

The operators $f_{n\sigma}$ ($f_{n\sigma}^{\dagger}$) correspond to the nth site of the Wilson chain, with exponentially decaying hopping matrix elements t_{n} between neighboring sites of the chain.[55] As a consequence, by adding consecutive sites, one is able to access transport at lower and lower energy scales. In this way the method generally provides a nonperturbative description of the crossover from a free magnetic impurity at high temperatures to a screened spin at low temperatures.[55] The Hamiltonian (8) can be solved iteratively by adding consecutive sites of the chain. This procedure allows for resolving static and dynamic properties of the system at energy scale $\Lambda^{-n/2}$, with n being a given iteration.

Since the NRG calculations may in general pose a serious numerical challenge, it becomes essential to take advantage of as many available symmetries of the system's Hamiltonian as possible. To efficiently address the present problem, we have employed the flexible density-matrix numerical renormalization-group (DM-NRG) code,[63] which can exploit an arbitrary number of both Abelian and non-Abelian symmetries.[64] In the case under discussion, the $U_{\text{charge}}(1) \times U_{\text{spin}}(1)$ symmetry of the model has been used, so that the zth component of the total spin,

$$\widetilde{S}_{z}^{t} = S_{z}^{t} + \frac{1}{2} \sum_{n=0}^{\infty} (f_{n\uparrow}^{\dagger} f_{n\uparrow} - f_{n\downarrow}^{\dagger} f_{n\downarrow}), \quad (9)$$

where $S_{z}^{t} = S_{z} + s_{z}$, as well as the total charge

$$\widetilde{Q}^{t} = \sum_{\sigma} c_{\sigma}^{\dagger} c_{\sigma} - 1 + \sum_{n=0}^{\infty} \left(\sum_{\sigma} f_{n\sigma}^{\dagger} f_{n\sigma} - 1 \right), \quad (10)$$

served as quantum numbers according to which the states of the Hamiltonian were classified during computation. Finally, the discretization parameter $\Lambda = 1.8$ has been taken in calculations, and we have kept 2000 states after each step of the iteration.

The central quantity of interest is the OL spin-dependent *spectral function*[55,65]

$$A_{\sigma}(\omega) = -\frac{1}{\pi} \text{Im} \langle\langle c_{\sigma} | c_{\sigma}^{\dagger} \rangle\rangle_{\omega}^{\text{r}}, \quad (11)$$

where $\langle\langle c_{\sigma} | c_{\sigma}^{\dagger} \rangle\rangle_{\omega}^{\text{r}}$ denotes the Fourier transform of the retarded Green's function $\langle\langle c_{\sigma} | c_{\sigma}^{\dagger} \rangle\rangle_{t}^{\text{r}} = -i\theta(t) \langle\{c_{\sigma}(t), c_{\sigma}^{\dagger}(0)\}\rangle$ of the orbital level. Some technical details concerning calculation of the spectral function can be found in Appendix A.

Having found the spectral function, one can determine the *linear-response conductance g* from the Landauer-Wingreen-Meir formula,[66–69] which at $T = 0$ yields

$$g = \pi \sum_{\sigma} \frac{2\Gamma_{\sigma}^{L} \Gamma_{\sigma}^{R}}{\Gamma_{\sigma}^{L} + \Gamma_{\sigma}^{R}} \cdot A_{\sigma}(\omega = 0) \quad \left(\text{in units of } \frac{2e^{2}}{h}\right), \quad (12)$$

with $\Gamma_{\uparrow(\downarrow)}^{L} = \frac{\Gamma}{2}(1 \pm P)$ and $\Gamma_{\uparrow(\downarrow)}^{R} = \frac{\Gamma}{2}(1 \pm P)$ for the *parallel* magnetic configuration of electrodes, while $\Gamma_{\uparrow(\downarrow)}^{L} = \frac{\Gamma}{2}(1 \pm P)$ and $\Gamma_{\uparrow(\downarrow)}^{R} = \frac{\Gamma}{2}(1 \mp P)$ for the *antiparallel* one. We assumed that both electrodes are made of the same material and P denotes their spin polarization. The effective coupling between the MQD and the reservoir for the *parallel* magnetic configuration is $\Gamma_{\uparrow(\downarrow)}^{\text{P}} = \Gamma(1 \pm P)$, while for the *antiparallel* one $\Gamma_{\uparrow(\downarrow)}^{\text{AP}} = \Gamma$, with $\Gamma = (\Gamma_{\uparrow} + \Gamma_{\downarrow})/2$. Note that in the case of left-right symmetric systems, $\Gamma_{\uparrow(\downarrow)}^{\text{AP}}$ is independent of σ in

the antiparallel configuration, and hence the system behaves effectively as coupled to nonmagnetic leads. As a result, the linear spin-resolved conductance (in units of $\frac{2e^2}{h}$) in the two magnetic configurations is given by

$$\begin{cases} g_{\uparrow(\downarrow)}^{\mathrm{P}} = \frac{\pi}{2}(1 \pm P)\Gamma A_{\uparrow(\downarrow)}^{\mathrm{P}}(\omega = 0), \\ g_{\uparrow(\downarrow)}^{\mathrm{AP}} = \frac{\pi}{2}(1 - P^2)\Gamma A_{\uparrow(\downarrow)}^{\mathrm{AP}}(\omega = 0), \end{cases} \qquad (13)$$

with $A_{\sigma}^{\mathrm{P/AP}}$ being the spectral function in the respective magnetic configuration.

III. NUMERICAL RESULTS AND DISCUSSION

Transport characteristics of the system, such as the linear-response conductance g and tunnel magnetoresistance (TMR), have been numerically calculated for a hypothetical MQD characterized by the spin number $S = 2$. Since the key feature of the transport regime under discussion is the presence of the Kondo resonance, it is convenient to introduce the Kondo temperature T_{K} as the most relevant energy scale for the system, to which other energy parameters will be related, if necessary. In the present work, the Kondo temperature T_{K} is estimated from the half width at half maximum of the Kondo resonance in spectral function at $T = 0$ for $J = 0$ and $P = 0$.[32,34] We note here that, for the sake of simplicity, we assume $k_{\mathrm{B}} \equiv 1$, i.e., temperatures are also given in units of energy. As a result, for the parameters used in Fig. 2, we get $T_{\mathrm{K}}/W \approx 5 \times 10^{-4}$ ($T_{\mathrm{K}}/\Gamma \approx 0.022$).

Before presenting and discussing numerical results, it is worth recalling that the Kondo effect appears as a result of spin-exchange processes in the OL due to its strong coupling to electrodes. This coupling is described here by the effective hybridization parameter Γ, which introduces the Kondo

temperature T_{K} as the relevant energy scale. However, the model considered provides also another independent physical mechanism (channel) through which the Kondo effect can be modified, i.e., the exchange interaction J between an electron in the OL and the MQD's magnetic core. Therefore one can expect the ratio of the J coupling and the Kondo temperature T_{K} to be the key parameter controlling whether or not the Kondo resonance will appear. Indeed, we show below that the electronic correlations between the OL and electrodes effectively result in the formation of the Kondo resonance only if $|J| \lesssim T_{\mathrm{K}}$. In order to see how the parameters of the system, especially the J coupling and the magnetic anisotropy D, influence the transport properties, we first calculate and discuss the relevant spectral functions.

A. Spectral functions

In the following we will analyze dependence of the spectral functions of the OL on some essential parameters of the system. Figure 2 shows the normalized spin-resolved spectral functions $\pi\Gamma_{\sigma}A_{\sigma}(\omega)$ as a function of the OL energy ε in the antiparallel and parallel magnetic configurations for $|J|/T_{\mathrm{K}} \approx 2$. In the antiparallel configuration the spectral functions for both spin components are equal. In the parallel configuration, on the other hand, the main contribution comes from the spin-up electrons, which are the majority ones. In both configurations and for both types of exchange coupling, the spectral functions show clear resonances associated with degeneracy of the neighboring charge states—compare the boundaries between regions corresponding to different Q, where Q denotes the average number of electrons occupying the OL. In the singly occupied regime, $Q = 1$, the Kondo effect due to hybridization of the OL spin with the conduction
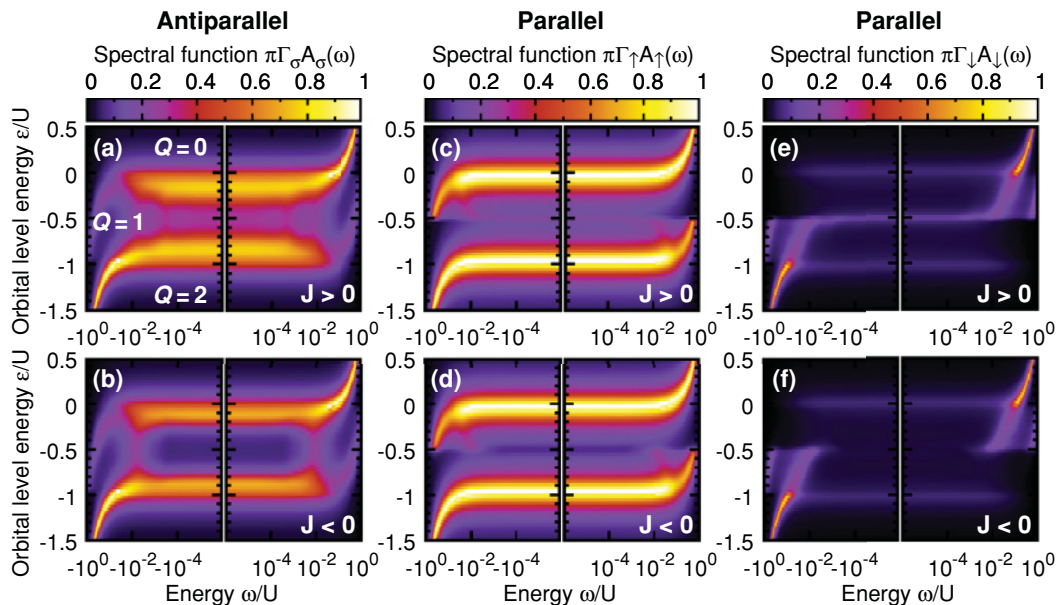

FIG. 2. (Color online) Normalized spin-resolved orbital level (OL) spectral functions, $\pi\Gamma_{\sigma}A_{\sigma}(\omega)$, shown as a function of the OL energy ε in the *antiparallel* (a),(b) and *parallel* (c)–(f) magnetic configurations. Top panel corresponds to the case of *ferromagnetic* ($J > 0$) coupling between electrons in the OL and MQD's magnetic core, while the bottom one presents results for the *antiferromagnetic* coupling. The variable Q denotes the average number of electrons occupying the OL. The parameters are $U/W = 0.3$, $D/U \approx 1.7 \times 10^{-4}$ ($D/T_{\mathrm{K}} = 0.1$), $\Gamma/U \approx 0.075$, $|J|/\Gamma \approx 0.044$ ($|J|/T_{\mathrm{K}} \approx 2$), $B_z = 0$, and $P = 0.5$. Note that the spectral functions are presented on a logarithmic scale.

electrons of the leads should be present. However, there are two ingredients that may generally suppress the Kondo resonance: the exchange coupling J and the exchange field due to the presence of ferromagnetic leads. Since the results in Fig. 2 are shown for $|J|/T_K \approx 2$, only the reminiscent of the Kondo effect can be observed. The suppression of the Kondo resonance is especially visible for the antiferromagnetic coupling ($J < 0$). Moreover, while in the case of ferromagnetic coupling ($J > 0$) some residual Kondo resonance can still be visible for the energy corresponding to the particle-hole symmetry ($\varepsilon = -U/2$), the resonance is practically absent for the antiferromagnetic coupling, though some side resonances appear. The origin of these additional features will be discussed further in the text.

Let us now analyze how the shape of spectral functions in the Kondo regime evolves when the exchange interaction between electrons in the OL and the MQD's core is turned on gradually; see Figs. 3(a)–3(f). Note that whenever we consider behavior of the system in the particle-hole symmetric point, i.e., for $\varepsilon = -U/2$, only the range of positive energies is presented. As one might expect, the behavior of the system for small values of $|J|$, i.e., $|J| \ll T_K$, resembles that of a single-level quantum dot, and a well defined and pronounced Kondo peak in the *antiparallel* configuration of the electrodes' magnetic moments is observed for $\omega \lesssim T_K$; see Figs. 3(a) and 3(b). In the *parallel* configuration, on the other hand, spin-dependent coupling to the electrodes acts as an effective exchange field[70] leading to spin splitting of the OL. This in turn results in suppression of the Kondo effect, except for the particle-hole symmetric point, $\varepsilon = -U/2$, as shown in Figs. 3(c)–3(f), where the effective exchange field vanishes. In the antiparallel configuration, the resultant coupling is the same for the spin up and spin down when the system is left-right symmetric. Consequently, there is no exchange field and we observe a well-pronounced peak in the spectral function at the Fermi level also outside the particle-hole symmetric point.[70–74]

The height of the Kondo peak becomes reduced with the increase of $|J|$, and for $|J| \gg T_K$ the peak almost completely vanishes. We note that the disappearance of the resonance is faster in the case of the antiferromagnetic coupling ($J < 0$); see Figs. 3(b), 3(d), and 3(f). Furthermore, as the J coupling grows, some additional features in the spectral functions emerge. Apart from the Hubbard peak originating from the Coulomb repulsion of two electrons in the OL, there are two additional resonances for $J > 0$, marked as dashed lines A and B in Fig. 3(a), and one resonance for $J < 0$, line C in Fig. 3(b). Interestingly, the position of one of the two resonances for $J > 0$ remains roughly independent of energy (line A), whereas the other resonance moves toward larger energies as J increases (line B); see Fig. 3(a).

Some insight into the physical origin of the resonances A, B, and C can be gained by considering the lowest energy states of a free-standing MQD with one extra electron in the OL; see Figs. 3(g) and 3(h).[75] First, we note that the consequence of exchange interaction between an electron in the OL and magnetic core is a decomposition of the molecular magnetic states into two spin multiplets, corresponding to $S + 1/2$ and $S - 1/2$. In addition, the sign of the coupling parameter J determines which of the two multiplets has lower
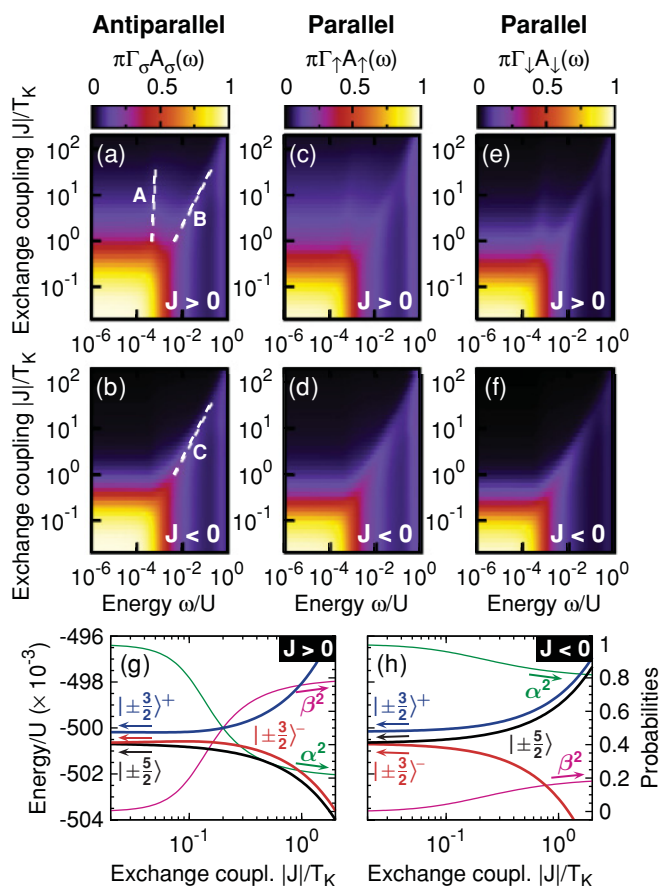

FIG. 3. (Color online) Normalized spin-resolved orbital level (OL) spectral functions shown for different values of the exchange parameter J in the case of (a),(c),(e) *ferromagnetic* ($J > 0$) and (b),(d),(f) *antiferromagnetic* ($J < 0$) coupling, and for $\varepsilon = -U/2$. The spectral function displays two additional resonances for $J > 0$, marked by dashed lines A and B, and a single resonance for $J < 0$, marked by dashed line C. The bottom panel (g),(h) illustrates the dependence of several lowest energy states of a singly occupied MQD on the parameter J (thick lines), and the corresponding probabilities of finding the electron in a certain spin state for $|\pm \frac{3}{2}\rangle^{\pm}$ (thin lines): $\alpha^2 \equiv (\mathbb{A}^+)^2 = (\mathbb{B}^-)^2$, while $\beta^2 \equiv (\mathbb{B}^+)^2 = (\mathbb{A}^-)^2$ [for details see Eq. (14) and the paragraph below it]. Remaining parameters as in Fig. 2.

energy. Since we focus exclusively on the case of $T = 0$, it is justified to take into account only the relevant low-energy states in both spin-multiplets. These are presented in Figs. 3(g) and 3(h), where the zero-field ($B_z = 0$) energy of states $|\pm \frac{5}{2}\rangle$, and $|\pm \frac{3}{2}\rangle^{\pm}$ is presented as a function of the coupling parameter J. The superscript $\pm$ at the states $|\pm \frac{3}{2}\rangle^{\pm}$ is used to distinguish between states of higher ($+$) and lower ($-$) energy. We note that the state $|\pm \frac{5}{2}\rangle$ belongs to the spin multiplet corresponding to $S + 1/2$, while for $J > 0$ the state $|\pm \frac{3}{2}\rangle^{-}$ belongs to the multiplet $S + 1/2$ and the state $|\pm \frac{3}{2}\rangle^{+}$ to the multiplet $S - 1/2$ (note that we assumed $S = 2$). For $J < 0$, the situation is opposite, i.e., $|\pm \frac{3}{2}\rangle^{-}$ belongs to the multiplet $S - 1/2$ whereas the state $|\pm \frac{3}{2}\rangle^{+}$ belongs to the multiplet

$S + 1/2$. In the absence of external magnetic field the MQD's states of interest take the form

$$\begin{cases} |S_z^t = \pm\tfrac{5}{2}\rangle = |\uparrow(\downarrow)\rangle_{OL} \otimes |\pm 2\rangle_{core}, \\ |S_z^t = -\tfrac{3}{2}\rangle^{\pm} = \mathbb{A}_{-3/2}^{\pm} |\downarrow\rangle_{OL} \otimes |-1\rangle_{core} \\ \qquad\qquad + \mathbb{B}_{-3/2}^{\pm} |\uparrow\rangle_{OL} \otimes |-2\rangle_{core}, \\ |S_z^t = +\tfrac{3}{2}\rangle^{\pm} = \mathbb{A}_{+3/2}^{\pm} |\uparrow\rangle_{OL} \otimes |+1\rangle_{core} \\ \qquad\qquad + \mathbb{B}_{+3/2}^{\pm} |\downarrow\rangle_{OL} \otimes |+2\rangle_{core}, \end{cases} \quad (14)$$

with $|\cdot\rangle_{OL(core)}$ denoting the spin state of OL (magnetic core). The coefficients $\mathbb{A}_m^{\pm} = \mathbb{A}^{\pm} \exp[i\phi_m^{\pm}]$ and $\mathbb{B}_m^{\pm} = \mathbb{B}^{\pm} \exp[i\gamma_m^{\pm}]$ can be regarded as effective Clebsch-Gordan coefficients, which are nontrivial functions of the system's parameters J and D.[75] Here, $\phi_m^{\pm}$ and $\gamma_m^{\pm}$ are relevant phase factors. As above, the superscript $\pm$ is used to distinguish between states of higher $(+)$ and lower $(-)$ energy. It is worth emphasizing that, to some extent, the situation under consideration is similar to the case of a quantum dot subjected to an external magnetic field, which leads to splitting of the Kondo resonance.[35,70] However, in the case of a simple quantum dot in a magnetic field there are two energy levels, whereas the energy structure of a MQD is much more complex, even in zero field. Moreover, except for the states $|\pm\tfrac{5}{2}\rangle$, all MQD's states for $Q = 1$ correspond to an electron in the OL being in the superposition of spin-up and spin-down states.

Let us now discuss cotunneling processes leading to the resonances for *ferromagnetic* (FM) exchange coupling ($J > 0$); see the top panel of Fig. 3. We emphasize that now we consider the regime of large J (i.e., $J > T_K$ and $J < \Gamma$), where the zero-energy resonance is absent and only side resonances (lines A and B) appear. Assume that initially the molecule occupies the state $|-\tfrac{5}{2}\rangle$. Due to spin-flip cotunneling processes, the MQD can be excited to one of the two states: $|-\tfrac{3}{2}\rangle^-$ (resonance A) and $|-\tfrac{3}{2}\rangle^+$ (resonance B); see Fig. 3(g). Taking into account the energy spectrum[75] one can estimate the corresponding energy gaps for $|J| \gg D$ as (exact formulas in Appendix B)

$$\begin{cases} \Delta_1^{FM} \approx 2SD\left[1 - \dfrac{2(|J| - D)}{(2S+1)(|J| - 2D)} \right], \\ \Delta_2^{FM} \approx \dfrac{2S+1}{2}|J|. \end{cases} \quad (15)$$

Thus the resonance corresponding to the line A in Fig. 3(a) is related to transitions characterized by the energy gap Δ_1^{FM}, while the resonance indicated by line B is associated with the gap Δ_2^{FM}. Moreover, one can note that Δ_2^{FM} depends linearly on J, whereas Δ_1^{FM} only slightly changes with J.

The picture presented above for $J > 0$ alters only slightly when the exchange coupling changes to the *antiferromagnetic* (AFM) one ($J < 0$); see Figs. 3(b), 3(d), and 3(f). The position of the spin multiplets $S + 1/2$ and $S - 1/2$ is now interchanged when compared to that for $J > 0$; Fig. 3(h). When the MQD is initially in the state $|-\tfrac{3}{2}\rangle^-$, then the spin-flip cotunneling processes can excite the MQD to one of the states: $|-\tfrac{5}{2}\rangle$ and $|-\tfrac{3}{2}\rangle^+$. Moreover, for $|J| \gg D$, the energy gaps associated with these transitions are roughly equal,

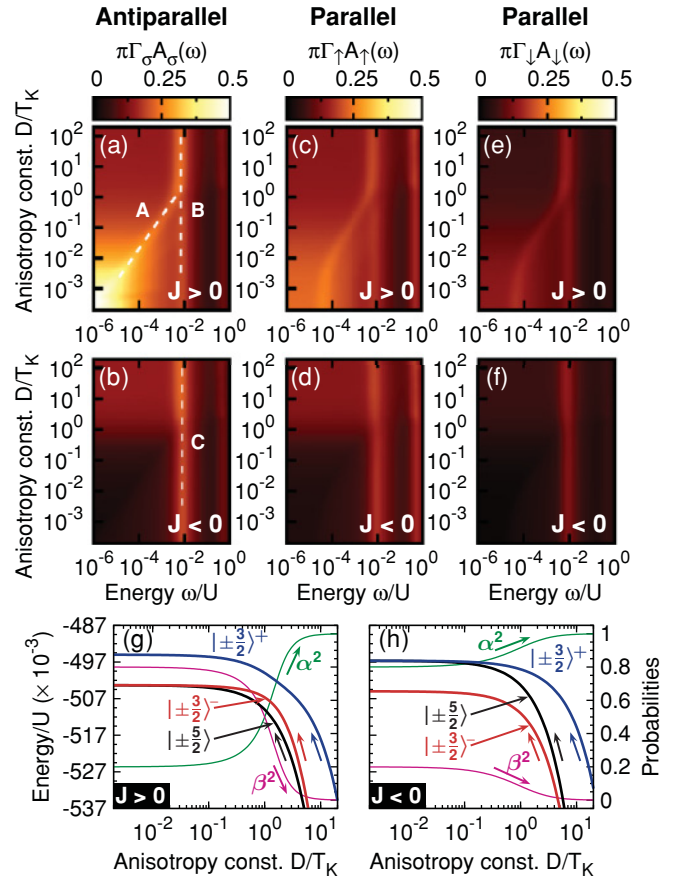$$\Delta_1^{AFM} \approx \Delta_2^{AFM} \approx \frac{2S+1}{2}|J|. \quad (16)$$

FIG. 4. (Color online) Similar as in Fig. 3, but now the dependence of the normalized spin-resolved spectral function on the uniaxial anisotropy constant D is presented for $|J|/T_K \approx 2$. A monochromatic color scheme is used here to highlight how the position of the resonances changes with varying D.

As a consequence, only the resonance denoted by line C is then visible in Fig. 3(b). The physical origin of the resonances in the parallel magnetic configuration, Figs. 3(c)–3(e) and 3(d)–3(f), can be accounted for in a qualitatively similar way. Finally, weak vertical lines visible in Fig. 3 for $\omega = U$ correspond to the resonance between singly occupied and empty OL.

As shown above, the exchange coupling of electrons in the OL and magnetic core modifies the energy spectrum of a MQD, and hence affects the Kondo effect. However, it has been demonstrated experimentally[14,20,45] that the energy spectrum can also be modified by changing the anisotropy constant D. Variation of the OL spectral functions with D is shown in Fig. 4 for a specific value of $|J|/T_K \approx 2$. Since $|J| > T_K$, the zero-energy Kondo resonance is practically absent, and only side resonances are visible. These resonances, marked in Figs. 4(a) and 4(b) by the letters A, B, and C, correspond to the relevant resonances in Figs. 3(a) and 3(b).

Especially interesting seems to be the case of $J > 0$, where two resonances (A and B) emerge at $D \approx T_K$. By a closer inspection of Fig. 4(g) one finds that this takes place when the condition $D \gg J/2$ is satisfied. However, it should be noted that according to our definition of the Kondo temperature, the relation $D = J/2 \approx T_K$ is only coincidental, and thus

valid just for the current set of parameters. Moreover, in the limit $D \gg |J|$ the energy gaps introduced above can be estimated as

$$
\begin{cases}
\Delta_1^{\text{FM}} \approx SJ - \dfrac{(2S+1)^2 J^2}{16(2S-1)D}, \\[2mm]
\Delta_2^{\text{FM}} \approx (2S-1)D + \dfrac{(2S+1)^2 J^2}{16(2S-1)D},
\end{cases}
\tag{17}
$$

so that Δ_1^{FM} is nearly constant with respect to D, whereas Δ_2^{FM} depends almost linearly on D. At first glance, the latter result appears to contradict the shape of the resonance B seen in Fig. 4(a), so that consideration of the energy spectrum becomes apparently insufficient. In order to account for this disparity, we must also take into account the explicit form of the MQD's states contributing to the resonances; see Eq. (14). For $D > |J|/2$, we have $(\mathbb{B}^-)^2 > (\mathbb{A}^-)^2$ and $(\mathbb{A}^+)^2 > (\mathbb{B}^+)^2$, and as the magnetic anisotropy D increases, at some point we get $(\mathbb{B}^-)^2 = (\mathbb{A}^+)^2 \approx 1$ and $(\mathbb{A}^-)^2 = (\mathbb{B}^+)^2 \approx 0$, Fig. 4(g), which basically means that $|-\frac{3}{2}\rangle^- \approx |\uparrow\rangle_{\text{OL}} \otimes |-2\rangle_{\text{core}}$ and $|-\frac{3}{2}\rangle^+ \approx |\downarrow\rangle_{\text{OL}} \otimes |-1\rangle_{\text{core}}$. In other words, when $D \gtrsim |J|$, the cotunneling processes associated with transitions between states $|-\frac{5}{2}\rangle$ and $|-\frac{3}{2}\rangle^-$ are allowed, while those between states $|-\frac{5}{2}\rangle$ and $|-\frac{3}{2}\rangle^+$ are forbidden. Consequently, the resonance marked with a vertical dashed line in Fig. 4(a) actually represents two independent resonances: B for $D \lesssim |J|$ and A for $D \gtrsim |J|$.

To complete the discussion of spectral functions, we note that the presence and behavior of resonance C for the antiferromagnetic J coupling ($J < 0$), Fig. 4(b), can be explained in a way similar to that for $J > 0$, with the relevant energy gaps for $D \gg |J|$ estimated as

$$
\begin{cases}
\Delta_1^{\text{AFM}} \approx S|J| + \dfrac{(2S+1)^2 J^2}{16(2S-1)D}, \\[2mm]
\Delta_2^{\text{AFM}} \approx (2S-1)D + \dfrac{(2S+1)^2 J^2}{8(2S-1)D}.
\end{cases}
\tag{18}
$$

However, only virtual spin-flip transitions between the states $|-\frac{3}{2}\rangle^-$ and $|-\frac{5}{2}\rangle$, and represented by the energy gap Δ_1^{AFM} [see Eq. (18)], are then possible. On the other hand, in the opposite limit, $D \ll |J|$, both types of spin-flip cotunneling processes characteristic for the antiferromagnetic J coupling (as discussed earlier) can in principle operate. Both these transitions are associated with the same energy gap given by Eq. (16), which, unlike in the case of $J > 0$, results in the formation of one resonance only; Fig. 4(b).

B. Conductance in the linear-response regime

From the spectral function discussed above one can determine the spin-resolved as well as total linear conductance, shown in Figs. 5(a)–5(g). For $|J| \ll T_K$, the results well known for the Kondo effect in a single-level quantum dot are recovered.[60,61,74] In particular, for the *antiparallel* magnetic configuration an enhanced conductance occurs in the blockade regime (single electron in the OL, $Q = 1$), whereas in the *parallel* configuration only a sharp peak in the particle-hole symmetry point, $\varepsilon = -U/2$, appears. More precisely, in the *antiparallel* configuration the linear conductance (measured in the units of $2e^2/h$) is given by $g^{\text{AP}} = 1 - P^2$, while

in the *parallel* configuration the conductance reaches unity for $\varepsilon = -U/2$, $g^P = 1$, with $g^{\text{P/AP}} = \sum_\sigma g_\sigma^{\text{P/AP}}$ representing the total linear conductance.[74,76] Suppression of the Kondo effect for other values of ε in the latter case is a consequence of spin splitting of the OL due to an effective exchange field created by ferromagnetic electrodes, as has already been mentioned in the previous section.

When the strength of the J coupling increases, the Kondo effect becomes gradually suppressed and the linear conductance in the blockade ($Q = 1$) region decreases.[76,77] In order to explain this dependence, we note that in the situation under discussion electrons are transmitted through OL that is exchange-coupled to the magnetic core; see Eqs. (14). As a result, cotunneling processes responsible for the Kondo state are more complex than in the case of $J = 0$. First, the amplitude of the cotunneling processes becomes reduced as now the electron occupying the OL is in a superposition of the spin-up and spin-down states. Second, the J coupling creates an energy gap between the relevant states, which effectively suppresses the Kondo effect.

Looking more carefully at the conductance curves in Fig. 5, one finds some difference between the cases with $J > 0$ and $J < 0$. While for $J < 0$ the Kondo peak vanishes rapidly after $|J|$ exceeds T_K, some remanent Kondo peak is still visible for $J > 0$. This disparity stems from different properties of quantum states taking part in the formation of the Kondo state for $J > 0$ and $J < 0$. First, when $|J| > T_K$, the ground-state energy of a singly occupied MQD is lower for $J < 0$ than for $J > 0$ [compare Figs. 3(g) and 3(h)]. Second, the ground state for $J < 0$ is a superposition of spin-up and spin-down states, which is not the case when $J > 0$. As a result, the cotunneling processes driving the Kondo effect are more effective for $J > 0$ than for $J < 0$, which leads to lower conductance for $J < 0$ as compared to $J > 0$.

From the previous subsection we know that the uniaxial magnetic anisotropy modifies electron states of a MQD, affecting thus the Kondo effect. This is shown explicitly in Figs. 6 and 7. As one can note in Fig. 6, conductance in the parallel magnetic configuration is rather insensitive to the anisotropy constant D—regardless of the type of exchange coupling J, see the filled points in Figs. 7(c) and 7(d), and certain weak dependence on the anisotropy constant D appears then in the particle-hole symmetry point $\varepsilon = -U/2$ (Kondo peak); see Figs. 7(a) and 7(b). This dependence, however, becomes weaker when the magnitude of exchange coupling increases. On the other hand, the role of anisotropy is more important in the case of antiparallel magnetic configuration (also for $\varepsilon \neq -U/2$), especially for $|J| \gtrsim T_K$; see the hollow points in Figs. 7(c) and 7(d).

Variation of the conductance with the anisotropy constant D depends on the sign of exchange parameter J. The conductance curves for $J > 0$ and $J < 0$ differ significantly only for $D \ll |J|/2$, while when D exceeds $|J|/2$, the difference becomes insignificant. Moreover, it should be noted that in the parallel configuration the conductance for $J > 0$ decreases with growing D, whereas for $J < 0$, one observes the opposite tendency; see Fig. 7. Such an overlap of the conductance curves for ferromagnetic and antiferromagnetic J coupling in the limit of large anisotropy constant D can be explained in a similar
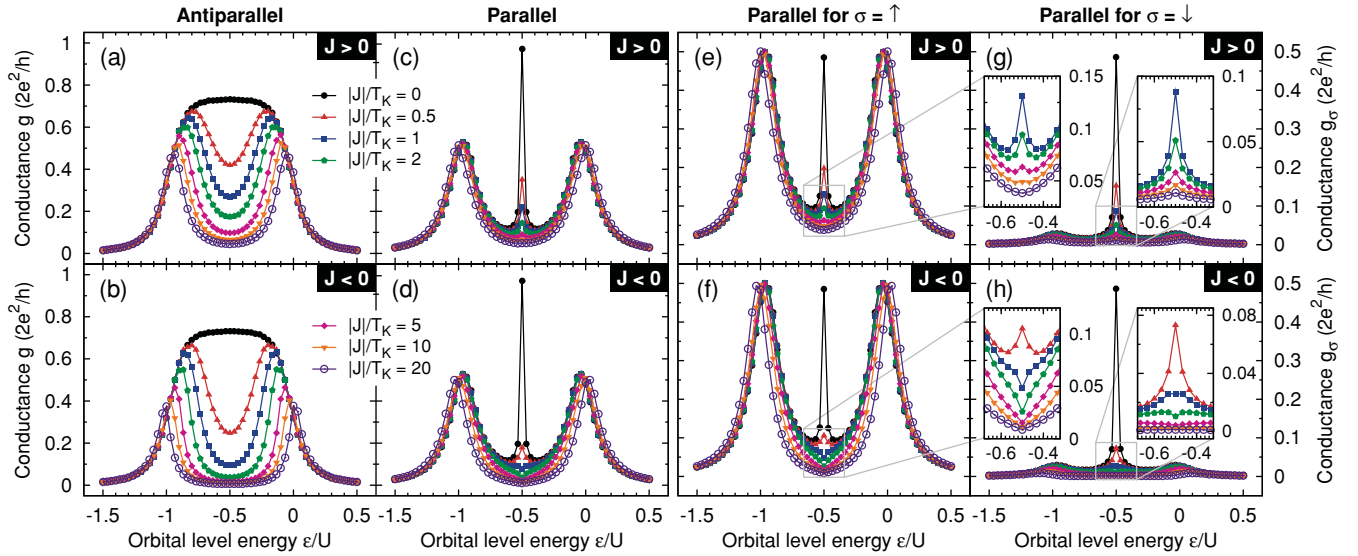
FIG. 5. (Color online) Total linear conductance $g = \sum_\sigma g_\sigma$ in the *antiparallel* (a),(b) and *parallel* (c),(d) magnetic configurations, and the spin-resolved linear conductance g_σ in the *parallel* configuration (e)–(h), presented as a function of the OL energy ε for indicated values of the parameter J in the case of the *ferromagnetic* ($J > 0$, top panel) and *antiferromagnetic* ($J < 0$, bottom panel) exchange interaction between electrons in the OL and magnetic core. All other parameters are as in Fig. 2.

way as above. One has to take into account that in the present situation the difference in energy gaps between ground states for $J > 0$ and $J < 0$ diminishes, and so do the energies of these states as D increases.

C. Tunnel magnetoresistance (TMR)

A quantity that describes the difference between transport properties in the *parallel* (P) and *antiparallel* (AP) magnetic

configurations is the *tunnel magnetoresistance* (TMR), defined here as[78]

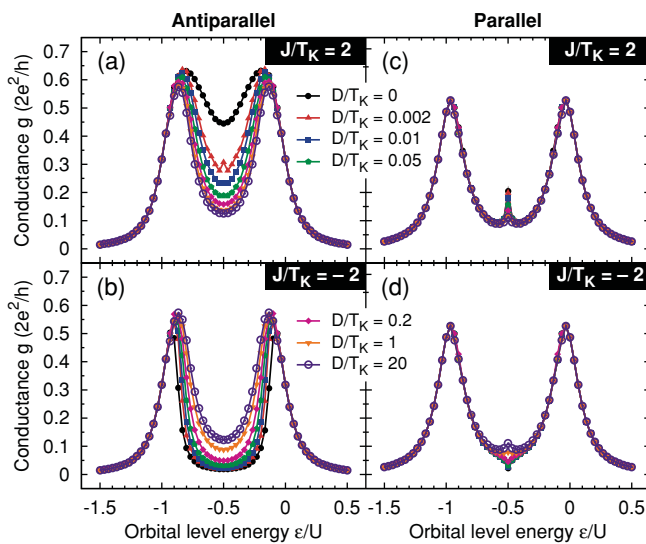$$\text{TMR} = \frac{g^P - g^{AP}}{g^{AP}}. \tag{19}$$

FIG. 6. (Color online) Influence of the uniaxial magnetic anisotropy D on the total linear conductance $g = \sum_\sigma g_\sigma$ for $|J|/T_K \approx 2$ and the exchange J coupling of either (a),(c) *ferromagnetic* ($J > 0$) or (b),(d) *antiferromagnetic* ($J < 0$) type. Other parameters are the same as in Fig. 2.
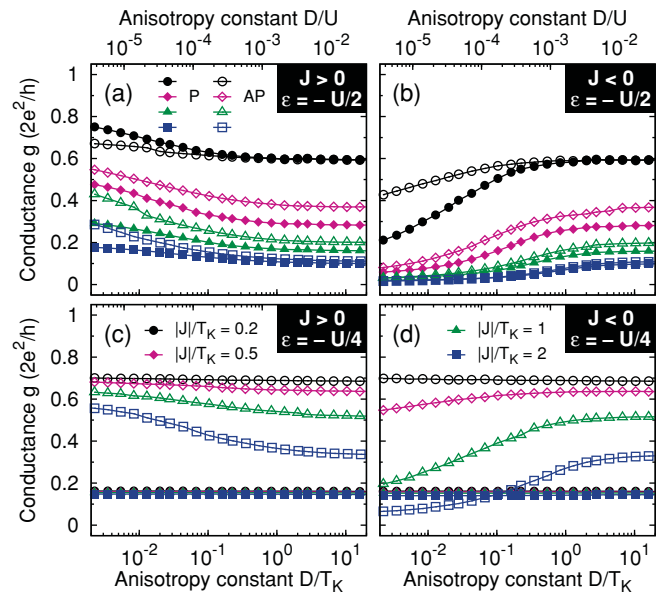

FIG. 7. (Color online) Total linear conductance $g = \sum_\sigma g_\sigma$ in the *parallel* (P:- filled points) and *antiparallel* (AP:- hollow points) magnetic configuration shown as a function of the uniaxial anisotropy constant D for indicated values of the J coupling and two representative OL energies: (a),(b) $\varepsilon = -U/2$ and (c),(d) $\varepsilon = -U/4$. Left panel corresponds to the *ferromagnetic* J coupling ($J > 0$), right panel to the *antiferromagnetic* one ($J < 0$). Other parameters as in Fig. 2.
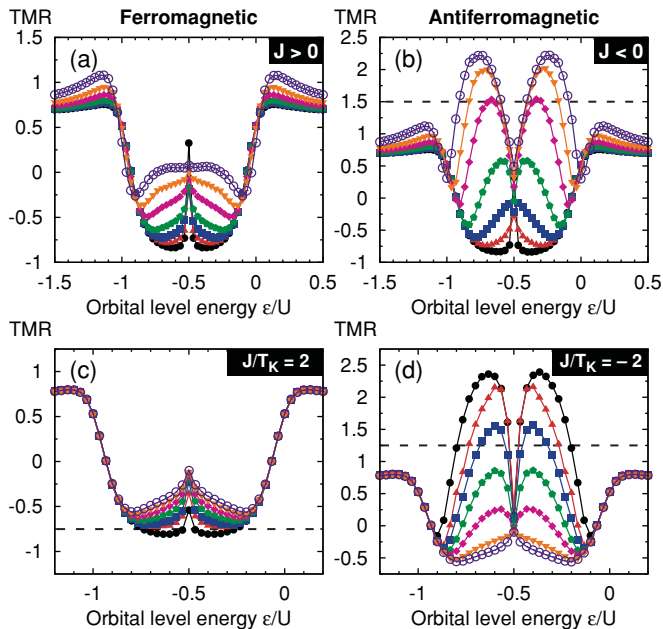
FIG. 8. (Color online) Tunnel magnetoresistance (TMR) presented as a function of the OL energy ε and the J coupling (a),(b) and the magnetic uniaxial anisotropy D (c),(d). Specific data points and parameters used in (a),(b) correspond to those in Fig. 5 and, analogously, in (c),(d) to Fig. 6. Dashed lines are introduced in order to facilitate comparison between TMR scales of adjacent plots for $J > 0$ and $J < 0$.

Using the conductance data analyzed in the previous subsection, we consider now how TMR depends on the key parameters of the model, i.e., on the J coupling, Figs. 8(a) and 8(b), and the magnetic anisotropy D, Figs. 8(c) and 8(d).

Let us first discuss the behavior of TMR as a function of the exchange coupling constant J, Figs. 8(a) and 8(b). Since for $|J| \ll T_K$ the conductance in the Kondo regime is generally larger in the antiparallel magnetic configuration than in the parallel one, regardless of the type of the J coupling, the corresponding TMR is negative in almost the entire Coulomb blockade region. The only exception occurs around the particle-hole symmetry point $\varepsilon = -U/2$.[76] This behavior follows from the suppression of the Kondo effect in the parallel configuration due to the exchange field, except for the particle-hole symmetric point. However, as $|J|$ becomes larger than T_K, the Kondo peak becomes suppressed also in the antiparallel configuration and positive TMR may be observed in the blockade regime as well. Moreover, suppression of the conductance g^{AP} for the antiparallel alignment is more evident in the case of *antiferromagnetic* ($J < 0$) coupling, Fig. 8(b), and the corresponding TMR is therefore significantly larger than for the *ferromagnetic* coupling ($J > 0$). Another observation for $J < 0$ is that when $|J| \gtrsim T_K$, two distinctive local maxima develop in the Coulomb blockade regime. Their positions depend on J and are symmetrical with respect to $\varepsilon = -U/2$. In addition, for $J < 0$, the TMR considerably surpasses the relevant Julliere's value, $2P^2/(1 - P^2)$,[78] which for the present parameters yields 2/3. Nonetheless, in the regions corresponding to empty or doubly occupied OL, one

always observes $g^P > g^{AP}$ with TMR approaching Julliere's value.[74]

Consider now variation of TMR with the magnetic anisotropy D; see Figs. 8(c) and 8(d). First of all, when the OL is either empty or occupied by two electrons, TMR remains insensitive to any changes in the anisotropy constant D. The same cannot be said about the region of ε corresponding to single occupation of the OL, where a large variation of TMR appears especially for $J < 0$; see Fig. 8(d). From Fig. 8(d) it follows that the smaller the magnetic anisotropy, the larger the TMR. The positions of the two local maxima in TMR, however, are now rather independent of D. Furthermore, for $D \ll |J|/2$, TMR stays positive. On the contrary, for the ferromagnetic J coupling ($J > 0$), Fig. 8(c), the TMR is negative in the considered range of ε and is only weakly modified upon changing D.

D. The restoring effect of magnetic field

In light of the foregoing discussion, we know that the Kondo effect is suppressed by exchange field generated by ferromagnetic electrodes as well as by the exchange coupling of the OL to magnetic core. Very recently, it was shown both experimentally and theoretically that one can compensate for the exchange-induced splitting of the orbital level by fine-tuning an external magnetic field, restoring thus the universal features of the Kondo effect.[79] Now we will thus consider the possibility of restoring the Kondo effect by applying a compensating external magnetic field B_c, oriented along the MQD's easy axis; see Fig. 9. The interesting observation worth mentioning is that the restoration can take place not only for the parallel magnetic configuration, Figs. 9(c) and 9(d), but also for the antiparallel one, Figs. 9(a) and 9(b). Furthermore, we would like to emphasize that the considered effect occurs only for the *antiferromagnetic* ($J < 0$) coupling between an electron in the OL and the MQD's magnetic core. From Figs. 9(c) and 9(d) it follows that for the parallel magnetic configuration the full unitary Kondo resonance (with the maximum value of conductance $g = 1$) is restored, whereas in the antiparallel configuration the peak of height $1 - P^2$ is retrieved owing to the magnetic field.

From the experimental point of view, it would be useful to know, at least roughly, how the magnitude of the compensating field B_c depends on the system's parameters. For this purpose, it is essential to know the physical mechanism responsible for the restoration of the Kondo effect. Thus in order to gain some deeper understanding of the problem, once again we employ the model of a free-standing MQD. It appears that the restoration of the Kondo effect becomes possible always when the magnetic field B_z brings the ground state of the spin multiplet $S_t = S - 1/2$ into resonance with the ground state of the multiplet $S_t = S + 1/2$. Depending on the direction of the field, the resonance takes place either between the states $|-\frac{3}{2}\rangle^- \leftrightarrow |-\frac{5}{2}\rangle$ or $|+\frac{3}{2}\rangle^- \leftrightarrow |+\frac{5}{2}\rangle$. Moreover, the possibility of such degeneracy is straightforwardly granted by the fact that these states are characterized by different numbers S_z^t (different zth component of the MQD's total spin). Accordingly, the Zeeman contributions to these states are different. Because the J coupling is of the *antiferromagnetic* type, the state with greater $|S_z^t|$ has then larger energy in the absence of magnetic
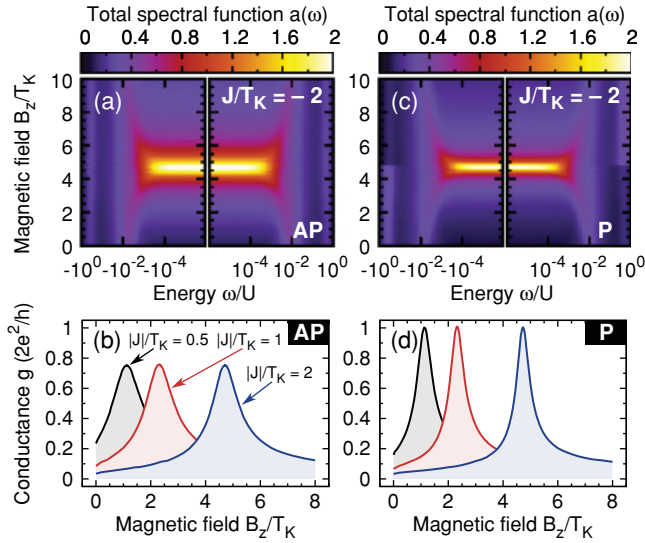
FIG. 9. (Color online) Restoration of the Kondo peak in the total spectral function $a(\omega) = \pi \sum_\sigma \Gamma_\sigma A_\sigma(\omega)$ (a),(c), and total conductance $g = \sum_\sigma g_\sigma$ (b),(d) by an external magnetic field B_z, shown for indicated values of the *antiferromagnetic J* coupling ($J < 0$) and for $\varepsilon = -U/2$. Left panel corresponds to the *antiparallel* (AP) magnetic configuration, right panel to the *parallel* (P) one. The other parameters as in Fig. 2.

field ($B_z = 0$). Thus if $B_z > 0$, the energy of the state $|-\frac{5}{2}\rangle$ decreases faster with increasing the field than the energy of $|-\frac{3}{2}\rangle^-$, so the degeneracy of these states occurs at a certain value of magnetic field, $B = B_c$, which can be then determined from the condition $\Delta_1^{AFM}(B_c) = 0$; see Fig. 10(a).

Taking into account the resonance condition introduced in the previous paragraph, we find the general expression describing dependence of the compensating field B_c on the J coupling and magnetic anisotropy D in the form

$$B_c = \frac{2S + 1}{4}|J| - \frac{2S - 1}{2}D$$
$$+ \sqrt{\frac{(2S + 1)^2}{16}J^2 + \frac{(2S - 1)^2}{4}D(D + |J|)}. \quad (20)$$

The comparison between the analytical solution and numerically derived values of the compensating field B_c for different magnetic configurations of the system is presented in Fig. 10(b). It is clearly visible that the numerical values of B_c generally follow the trend of the approximate analytical curve, Eq. (20), and substantial discrepancies arise only for small values of $|J|$, as one might expect. The slightly smaller value of the compensating field in the situation of a MQD attached to magnetic electrodes can be attributed to renormalization of MQD's energy levels due to the strong OL-electrodes coupling, which results in diminishing energy gaps between the states participating in the formation of the Kondo effect. It should be here emphasized that this difference can be seen only due to specific normalization of the compensating field B_c with respect to $|J|$. Otherwise, when presented in the logarithmic scale, the curves corresponding to numerical and analytical solutions follow the same trend; see the inset in Fig. 10(b).
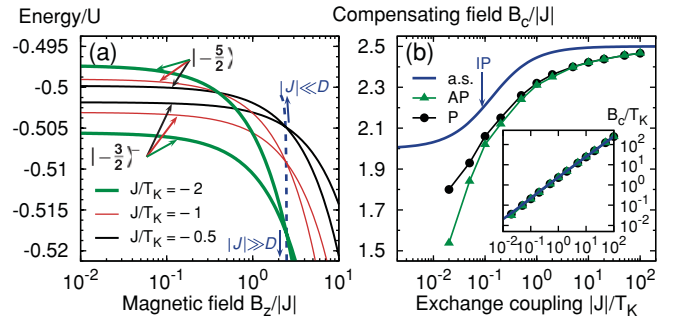

FIG. 10. (Color online) (a) Energies of ground states $|-\frac{5}{2}\rangle$ and $|-\frac{3}{2}\rangle^-$ shown as functions of an external magnetic field B_z for indicated values of the exchange coupling parameter J and for $D/U \approx 1.7 \times 10^{-4}$ ($D/T_K = 0.1$) and $\varepsilon = -U/2$. Dashed line corresponds to the analytical solution given by Eq. (20). (b) Dependence of the compensating field B_c on the value of the J coupling. Points represent numerical results obtained for the *antiparallel* (AP) and *parallel* (P) magnetic configuration, while the bold line delineates the analytical solution (a.s.), Eq. (20). IP indicates the inflexion point of the curve $B_c(|J|)$. Inset: the compensating field B_c normalized to T_K, shown on the logarithmic scale. Other parameters as in Fig. 2.

Finally, since the form of Eq. (20) is exactly the same as for Δ_1^{AFM}, Eq. (B2), the asymptotic values of B_c are immediately obtained as $B_c \approx (2S + 1)|J|/2$ for $|J| \gg D$, and $B_c \approx S|J|$ for $|J| \ll D$. Additionally, it might be helpful to know how the change of magnetic anisotropy D influences the analytical solution $B_c(|J|)$; see the bold line in Fig. 10(b). For this purpose, we calculate the inflexion point position (IPP) of the compensating magnetic-field curve $B_c(|J|)$,

$$\text{IPP} = \frac{2(2S - 1)}{(2S + 1)^2}[1 - (2S)^{2/3}][1 + (2S)^{1/3}]D. \quad (21)$$

It turns out that IPP depends linearly on D, with the proportionality constant being a complex function of the MQD's core spin number S. Consequently, modification of the magnetic anisotropy constant D does not affect the general shape of the compensating field curve $B_c(|J|)$, but it only leads to shifting of the curve's inflexion point.

IV. SUMMARY AND CONCLUSIONS

In this paper we have investigated transport properties in the Kondo regime of a class of systems exhibiting uniaxial magnetic anisotropy. The model assumed includes one orbital level through which electrons can tunnel and which is additionally exchange-coupled to a magnetic moment. The model can describe a single-level quantum dot in which electrons are exchange-coupled to an embedded magnetic impurity. It can also be used to describe transport through magnetic atoms and molecules.

Using the numerical renormalization-group method we have calculated spectral density of the OL level and linear conductance of the system. The key new feature of transport characteristics is the suppression of the Kondo effect by exchange coupling to the magnetic core. Independently of the sign of the coupling parameter J, suppression takes place for both ferromagnetic as well as antiferromagnetic coupling. In

the limit of small J, $|J| \ll T_K$, we find the Kondo resonance characteristic of single-level dots. This resonance is suppressed with increasing J but then some side resonances appear in the spectral density. It is worthy to note that the suppression of the Kondo peak in the case considered appears gradually with increasing J, contrary to the case of a dot exchange-coupled to electron reservoir of continuous density of states, where the suppression is associated with a quantum phase transition.[80]

We have also shown that the suppressed Kondo resonance in the spectral function and in transport characteristics can be restored by application of an external magnetic field. This restoration is, however, complete only in the case of antiferromagnetic exchange coupling ($J < 0$) for both the parallel and antiparallel magnetic configurations.

APPENDIX A: CALCULATION OF THE SPECTRAL FUNCTION

During the course of NRG iterative calculation, the spectral function $A_\sigma(\omega)$ is obtained as a set of the Dirac δ functions $\delta(\omega - \omega_n)$ at frequencies ω_n, which next have to be broadened in order to acquire a continuous spectrum. Because of logarithmic discretization of the conduction band, it is convenient to collect the δ peaks in logarithmic bins and broaden them using a logarithmic Gaussian distribution, with the broadening parameter typically given by $\log(\Lambda)$.[65,81,82] It turns out, however, that due to logarithmic discretization of the band and truncation during the NRG run, the broadened spectral function may exhibit some artifacts, such as an oscillatory behavior for energies smaller than the Kondo temperature. One of the tricks to overcome these problems is the so-called *self-energy trick*.[82,83]

The essential idea of the *self-energy trick* relies on finding the spectral function by constructing the full self-energy $\Sigma_\sigma(\omega)$ of the system.[83] The self-energy can be expressed as a ratio of two spectral functions. Although each spectral function displays similar problems related with discretization, by calculating their ratio one obtains a smooth function where most of the artifacts are suppressed. Having found the self-energy, one can then calculate the retarded Green's function $\langle\langle c_\sigma | c_\sigma^\dagger \rangle\rangle_\omega^r$ of the OL, Eq. (11), using the equation of motion method,[69]

$$\langle\langle c_\sigma | c_\sigma^\dagger \rangle\rangle_\omega^r = \frac{1}{\omega - \varepsilon_\sigma - \Sigma_\sigma^r(\omega)}, \tag{A1}$$

where $\varepsilon_\sigma = \varepsilon + \frac{1}{2}B_z(\delta_{\sigma\uparrow} - \delta_{\sigma\downarrow})$. The total self-energy consists of three terms,

$$\Sigma_\sigma^r(\omega) = \Sigma_\sigma^{Ur}(\omega) + \Sigma_\sigma^{Jr}(\omega) + \Delta_\sigma^r(\omega), \tag{A2}$$

which represent contributions stemming from the Coulomb interaction $\Sigma_\sigma^{Ur}(\omega)$, the exchange interaction between an electron spin in the OL and the core spin of the MQD, $\Sigma_\sigma^{Jr}(\omega)$, and the tunneling coupling of the OL to electrodes, $\Delta_\sigma^r(\omega)$. The explicit forms of the above self-energy contributions are given by

$$\Sigma_\sigma^{Ur}(\omega) = U \frac{\langle\langle n_{\bar{\sigma}} c_\sigma | c_\sigma^\dagger \rangle\rangle_\omega^r}{\langle\langle c_\sigma | c_\sigma^\dagger \rangle\rangle_\omega^r}, \tag{A3}$$

$$\Sigma_\sigma^{Jr}(\omega) = -\frac{J}{2}\left[\delta_{\sigma\uparrow} \frac{\langle\langle c_{\bar{\sigma}} S_- | c_\sigma^\dagger \rangle\rangle_\omega^r}{\langle\langle c_\sigma | c_\sigma^\dagger \rangle\rangle_\omega^r} + \delta_{\sigma\downarrow} \frac{\langle\langle c_{\bar{\sigma}} S_+ | c_\sigma^\dagger \rangle\rangle_\omega^r}{\langle\langle c_\sigma | c_\sigma^\dagger \rangle\rangle_\omega^r} \right.$$
$$\left. + (\delta_{\sigma\uparrow} - \delta_{\sigma\downarrow}) \frac{\langle\langle c_\sigma S_z | c_\sigma^\dagger \rangle\rangle_\omega^r}{\langle\langle c_\sigma | c_\sigma^\dagger \rangle\rangle_\omega^r} \right], \tag{A4}$$

$$\Delta_\sigma^r(\omega) = \frac{\Gamma_\sigma}{\pi}\left[\ln\left|\frac{W + \omega}{W - \omega}\right| - i\pi \right]. \tag{A5}$$

Finally, the *improved* spectral function of the orbital level is given by

$$A_\sigma(\omega) = -\frac{1}{\pi} \cdot \frac{\text{Im}\Sigma_\sigma^r(\omega)}{\left[\omega - \varepsilon_\sigma - \text{Re}\Sigma_\sigma^r(\omega)\right]^2 + \left[\text{Im}\Sigma_\sigma^r(\omega)\right]^2}. \tag{A6}$$

APPENDIX B: ENERGY GAPS

In the case of the *ferromagnetic* (FM) J coupling ($J > 0$), exact analytical expressions for the energy gaps Δ_1^{FM} and Δ_2^{FM} can be derived as the energy difference between appropriate MQD's states: $|\pm\frac{5}{2}\rangle$ and $|\pm\frac{3}{2}\rangle^-$ for Δ_1^{FM}, and $|\pm\frac{5}{2}\rangle$ and $|\pm\frac{3}{2}\rangle^+$ for Δ_2^{FM},[75] so that

$$\Delta_{1(2)}^{FM} = \frac{2S+1}{4}|J| + \frac{2S-1}{2}D$$
$$\mp \sqrt{\frac{(2S+1)^2}{16}J^2 + \frac{(2S-1)^2}{4}D(D-|J|)}. \tag{B1}$$

The energy gaps for *antiferromagnetic* (AFM) J coupling ($J < 0$) can be found in a similar way. The energy difference between the MQD's states $|\pm\frac{3}{2}\rangle^-$ and $|\pm\frac{5}{2}\rangle$ is then given by

$$\Delta_1^{AFM} = \frac{2S+1}{4}|J| - \frac{2S-1}{2}D$$
$$+ \sqrt{\frac{(2S+1)^2}{16}J^2 + \frac{(2S-1)^2}{4}D(D+|J|)}, \tag{B2}$$

whereas the formula for the gap between the states $|\pm\frac{3}{2}\rangle^-$ and $|\pm\frac{3}{2}\rangle^+$ takes the form

$$\Delta_2^{AFM} = 2\sqrt{\frac{(2S+1)^2}{16}J^2 + \frac{(2S-1)^2}{4}D(D+|J|)}. \tag{B3}$$

*misiorny@amu.edu.pl

[1] C. Joachim, J. K. Gimzewski, and A. Aviram, Nature (London) **408**, 541 (2000).

[2] S. Tans, A. Verschueren, and C. Dekker, Nature (London) **393**, 49 (1998).

[3] H. Park, J. Park, A. Lim, E. Andeson, A. Alivisatos, and P. McEuen, Nature (London) **407**, 57 (2000).

[4] J. Heath and M. Ratner, Phys. Today **56**(5), 43 (2003).

[5] P. Piva, G. DiLabio, J. Pitters, J. Zikovsky, M. Rezeq, S. Dogel, W. Hofer, and R. Wolkow, Nature (London) **435**, 658 (2005).

[6] L. Bogani and W. Wernsdorfer, Nat. Mater. **7**, 179 (2008).

[7] J. Green, J. Choi, A. Boukai, Y. Bunimovich, E. Johnston-Halperin, E. DeIonno, Y. Luo, B. Sheriff, K. Xu, Y. Shin, H.-R. Tseng, J. Stoddart, and J. Heath, Nature (London) **445**, 414 (2007).

[8] M. Mannini, F. Pineider, P. Sainctavit, C. Danieli, E. Otero, C. Sciancalepore, A. Talarico, M. Arrio, A. Cornia, D. Gatteschi, and R. Sessoli, Nat. Mater. **8**, 194 (2009).

[9] S. Loth, K. von Bergmann, M. Ternes, A. Otte, C. Lutz, and A. Heinrich, Nat. Phys. **6**, 340 (2010).

[10] M. Mannini, F. Pineider, C. Danieli, F. Totti, L. Sorace, P. Sainctavit, M.-A. Arrio, E. Otero, L. Joly, J. C. Cezar, A. Cornia, and R. Sessoli, Nature (London) **468**, 417 (2010).

[11] P. Gambardella, S. Rusponi, M. Veronese, S. Dhesi, C. Grazioli, A. Dallmeyer, I. Cabria, R. Zeller, P. Dederichs, K. Kern, C. Carbone, and H. Brune, Science **300**, 1130 (2003).

[12] C. Hirjibehedin, C. Lin, A. Otte, M. Ternes, C. Lutz, B. Jones, and A. Heinrich, Science **317**, 1199 (2007).

[13] F. Meier, L. Zhou, J. Wiebe, and R. Wiesendanger, Science **320**, 82 (2008).

[14] A. Otte, M. Ternes, K. von Bergmann, S. Loth, H. Brune, C. Lutz, C. Hirjibehedin, and A. Heinrich, Nat. Phys. **4**, 847 (2008).

[15] H. Brune and P. Gambardella, Surf. Sci. **603**, 1812 (2009).

[16] D. Gatteschi, R. Sessoli, and J. Villain, *Molecular Nanomagnets* (Oxford University Press, New York, 2006).

[17] H. B. Heersche, Z. de Groot, J. A. Folk, H. S. J. van der Zant, C. Romeike, M. R. Wegewijs, L. Zobbi, D. Barreca, E. Tondello, and A. Cornia, Phys. Rev. Lett. **96**, 206801 (2006).

[18] M.-H. Jo, J. E. Grose, K. Baheti, M. M. Deshmukh, J. J. Sokol, E. M. Rumberger, D. N. Hendrickson, J. R. Long, H. Park, and D. C. Ralph, Nano Lett. **6**, 2014 (2006).

[19] S. Voss, O. Zander, M. Fonin, U. Rüdiger, M. Burgert, and U. Groth, Phys. Rev. B **78**, 155403 (2008).

[20] A. Zyazin, J. van den Berg, E. Osorio, H. van der Zant, N. Konstantinidis, M. Leijnse, M. Wegewijs, F. May, W. Hofstetter, C. Danieli, and A. Cornia, Nano Lett. **10**, 3307 (2010).

[21] F. Elste and C. Timm, Phys. Rev. B **73**, 235305 (2006).

[22] C. Timm and F. Elste, Phys. Rev. B **73**, 235304 (2006).

[23] M. Misiorny and J. Barnaś, Phys. Rev. B **75**, 134425 (2007).

[24] M. Misiorny and J. Barnaś, Phys. Status Solidi B **246**, 695 (2009).

[25] M. Misiorny, I. Weymann, and J. Barnaś, Phys. Rev. B **79**, 224420 (2009).

[26] F. Delgado, J. J. Palacios, and J. Fernández-Rossier, Phys. Rev. Lett. **104**, 026601 (2010).

[27] H.-Z. Lu, B. Zhou, and S.-Q. Shen, Phys. Rev. B **79**, 174419 (2009).

[28] S. Barraza-Lopez, K. Park, V. García-Suárez, and J. Ferrer, Phys. Rev. Lett. **102**, 246801 (2009).

[29] L. Zhu, K. Yao, and Z. Liu, Appl. Phys. Lett. **96**, 082115 (2010).

[30] H. Hao, X. Zheng, Z. Dai, and Z. Zeng, Appl. Phys. Lett. **96**, 192112 (2010).

[31] M. Misiorny, I. Weymann, and J. Barnaś, Europhys. Lett. **89**, 18003 (2010).

[32] A. C. Hewson, *The Kondo Problem to Heavy Fermions* (Cambridge University Press, Cambridge, England, 1997).

[33] L. Kouwenhoven and L. Glazman, Phys. World **14**(1), 33 (2001).

[34] M. Ternes, A. Heinrich, and W.-D. Schneider, J. Phys.: Condens. Matter **21**, 053001 (2009).

[35] D. Goldhaber-Gordon, H. Shtrikman, D. Mahalu, D. Abusch-Magder, U. Meirav, and M. Kastner, Nature (London) **391**, 156 (1998).

[36] S. Cronenwett, T. Oosterkamp, and L. Kouwenhoven, Science **281**, 540 (1998).

[37] S. Sasaki, S. De Franceschi, J. Elzerman, W. Van der Wiel, M. Eto, S. Tarucha, and L. Kouwenhoven, Nature (London) **405**, 764 (2000).

[38] V. Madhavan, W. Chen, T. Jamneala, M. Crommie, and N. Wingreen, Science **280**, 567 (1998).

[39] J. Li, W. D. Schneider, R. Berndt, and B. Delley, Phys. Rev. Lett. **80**, 2893 (1998).

[40] J. Nygård, D. Cobden, and P. Lindelof, Nature (London) **408**, 342 (2000).

[41] J. Park, A. Pasupathy, J. Goldsmith, C. Chang, Y. Yaish, J. Petta, M. Rinkoski, J. Sethna, H. Abruña, P. McEuen, and D. Ralph, Nature (London) **417**, 722 (2002).

[42] W. Liang, M. Shores, M. Bockrath, J. Long, and H. Park, Nature (London) **417**, 725 (2002).

[43] L. Yu and D. Natelson, Nano Lett. **4**, 79 (2004).

[44] A. N. Pasupathy, R. C. Bialczak, J. Martinek, J. E. Grose, L. A. K. Donev, P. L. McEuen, and D. C. Ralph, Science **306**, 86 (2004).

[45] J. Parks, A. Champagne, T. Costi, W. Shum, A. Pasupathy, E. Neuscamman, S. Flores-Torres, P. Cornaglia, A. Aligia, C. Balseiro, G.-L. Chan, H. Abruña, and D. Ralph, Science **328**, 1370 (2010).

[46] C. Romeike, M. R. Wegewijs, W. Hofstetter, and H. Schoeller, Phys. Rev. Lett. **96**, 196601 (2006).

[47] C. Romeike, M. R. Wegewijs, W. Hofstetter, and H. Schoeller, Phys. Rev. Lett. **97**, 206601 (2006).

[48] M. N. Leuenberger and E. R. Mucciolo, Phys. Rev. Lett. **97**, 126601 (2006).

[49] G. Gonzalez, M. N. Leuenberger, and E. R. Mucciolo, Phys. Rev. B **78**, 054445 (2008).

[50] D. Roosen, M. R. Wegewijs, and W. Hofstetter, Phys. Rev. Lett. **100**, 087201 (2008).

[51] M. R. Wegewijs, C. Romeike, H. Schoeller, and W. Hofstetter, New J. Phys. **9**, 344 (2007).

[52] R.-Q. Wang and D. Y. Xing, Phys. Rev. B **79**, 193406 (2009).

[53] F. Elste and C. Timm, Phys. Rev. B **81**, 24421 (2010).

[54] K. G. Wilson, Rev. Mod. Phys. **47**, 773S (1975).

[55] R. Bulla, T. Costi, and T. Pruschke, Rev. Mod. Phys. **80**, 395 (2008).

[56] M. Mannini, F. Pineider, P. Sainctavit, L. Joly, A. Fraile-Rodríguez, M. Arrio, C. dit Moulin, W. Wernsdorfer, A. Cornia, D. Gatteschi, and R. Sessoli, Adv. Mater. **21**, 167 (2009).

[57] L. I. Glazman and M. E. Raikh, JETP Lett. **47**, 452 (1988).

[58] T. K. Ng and P. A. Lee, Phys. Rev. Lett. **61**, 1768 (1988).

[59] H. Bruus and K. Flensberg, *Many-body Quantum Theory in Condensed Matter Physics*, Oxford Graduate Texts (Oxford University Press, New York, 2004).

[60] M. S. Choi, D. Sánchez, and R. López, Phys. Rev. Lett. **92**, 56601 (2004).

[61]M. Sindel, L. Borda, J. Martinek, R. Bulla, J. König, G. Schön, S. Maekawa, and J. von Delft, Phys. Rev. B **76**, 45321 (2007).

[62]H. R. Krishna-murthy, J. W. Wilkins, and K. G. Wilson, Phys. Rev. B **21**, 1003 (1980).

[63]O. Legeza, C. Moca, A. Tóth, I. Weymann, and G. Zaránd, "Manual for the flexible DM-NRG code", e-print arXiv:0809.3143 (2008) (the code is available at [http://www.phy.bme.hu/~dmnrg/]).

[64]A. I. Tóth, C. P. Moca, O. Legeza, and G. Zaránd, Phys. Rev. B **78**, 245109 (2008).

[65]T. Costi, A. Hewson, and V. Zlatić, J. Phys.: Condens. Matter **6**, 2519 (1994).

[66]R. Landauer, Philos. Mag. **21**, 863 (1970).

[67]Y. Meir, N. S. Wingreen, and P. A. Lee, Phys. Rev. Lett. **66**, 3048 (1991).

[68]Y. Meir and N. S. Wingreen, Phys. Rev. Lett. **68**, 2512 (1992).

[69]H. Haug and A.-P. Jauho, *Quantum Kinetics in Transport and Optics of Semiconductors,* Springer Series in Solid-State Sciences Vol. 123 (Springer, New York, 1998).

[70]J. Martinek, Y. Utsumi, H. Imamura, J. Barnaś, S. Maekawa, J. König, and G. Schön, Phys. Rev. Lett. **91**, 127203 (2003).

[71]R. Świrkowicz, M. Wilczyński, and J. Barnaś, J. Phys.: Condens. Matter **18**, 2291 (2006).

[72]R. Świrkowicz, M. Wilczyński, M. Wawrzyniak, and J. Barnaś, Phys. Rev. B **73**, 193312 (2006).

[73]J. Barnaś and I. Weymann, J. Phys.: Condens. Matter **20**, 423202 (2008).

[74]I. Weymann, Phys. Rev. B **83**, 113306 (2011).

[75]Analytical expressions describing energies and corresponding states of the systems represented by the Hamiltonian (2) can be found in Refs. 22 and 24. Note, however, that the notation used in the present paper differs from the notation employed in the aforementioned articles.

[76]M. Misiorny, I. Weymann, and J. Barnaś, Phys. Rev. Lett. **106**, 126602 (2011).

[77]M. Misiorny, I. Weymann, and J. Barnaś, J. Appl. Phys. **109**, 07C732 (2011).

[78]M. Julliere, Phys. Lett. A **54**, 225 (1975).

[79]M. Gaass, A. K. Hüttel, K. Kang, I. Weymann, J. von Delft, and Ch. Strunk, e-print arXiv:1104.5699 (to be published).

[80]I. Weymann and J. Barnaś, Phys. Rev. B **81**, 35331 (2010).

[81]O. Sakai, Y. Shimizu, and T. Kasuya, J. Phys. Soc. Jpn. **58**, 3666 (1989).

[82]R. Žitko and T. Pruschke, Phys. Rev. B **79**, 85106 (2009).

[83]R. Bulla, A. Hewson, and T. Pruschke, J. Phys.: Condens. Matter **10**, 8365 (1998).